Periodic Orbit Theory: A Study of The Rössler Attractor

Joachim Mathiesen
Cpr-nr: 190476-xxxx

26.01.00

Abstract

The present text treats various aspects of the Rössler nonlinear equation system.

The leading Lyapunov exponent is calculated to clarify the chaotic behaviour of the system. The exponent is calculated numerically, first, integrating the equation system directly, and secondly, at the end of the text, using the periodic orbit theory. Symbolic dynamics including kneading theory is applied to find the admissible orbits of the system. The topological entropy of a return map is calculated using the topological ζ-function.

Term paper for the course Fysik711B fall semester 1999

1 The Rössler System

1.1 Trajectories and Stability

In general a nonlinear system of differential equations is written as,

$$\dot{\mathbf{x}} = \mathbf{v}(\mathbf{x}) \tag{1}$$

such that the tangent vector to the solution curve, the velocity field $\dot{\mathbf{x}}$, is equal to the vector field $\mathbf{v}$ evaluated at the local value $\mathbf{x}$. The solution curve to an initial point $\mathbf{x}_0$, the flow, is denoted by $\phi^t(\mathbf{x}_0) =: \mathbf{x}(t)$. The set $\{\phi^t(\mathbf{x}_0)|t \geq 0\}$ is called the orbit or the trajectory starting at $\mathbf{x}_0$. Trajectories in the present text are all found with the application of the fourth order Runge-Kutta algorithm.

For purposes of chaotic physics it is not convenient to consider solution curves of initial points individually. Individual points are "non-existing" behind glasses of finite precision and systems showing noticeable sensitivity on initial conditions thus are unpredictable over larger time scales. In order to set up time scales of predictability we extent our considerations to neighborhoods of initial points, i.e. swarms of surrounding points. In particular the temporal evolution of the initial point $\mathbf{x}_0$ is compared to the evolution of x_0 perturbed by an initial infinitesimal displacement η_0, $\mathbf{x}_0 + \eta_0$.

The evolution of the quantity $|\eta(t)|/|\eta_0|$, where $\eta(t) := \phi^t(\mathbf{x}_0 + \eta_0) - \phi^t(x_0)$, is described in terms of Lyapunov exponents. The Lyapunov exponent λ is defined as the limit

$$\lambda := \lim_{t\to\infty} \frac{1}{t} \ln \frac{|\eta(t)|}{|\eta_0|} \tag{2}$$

For practical purposes we make a little rewriting of the definition. First we make the following Taylor expansion to linear order

$$\eta(t) + \mathbf{x}(t) = \phi^t(\mathbf{x}_0 + \eta_0) \approx \phi^t(\mathbf{x}_0) + \mathbf{J}^t(\mathbf{x}_0)\eta_0 \tag{3}$$

where $\mathbf{J}^t$ is the Jacobian matrix,

$$\mathbf{J}^t_{ij}(\mathbf{x}_0) := \left.\frac{\partial \phi^t_i(\mathbf{x})}{\partial x_j}\right|_{\mathbf{x}=\mathbf{x}_0} \tag{4}$$

and see that the linearized neighbourhood changes with the Jacobian,

$$\eta(t) = \mathbf{J}^t(\mathbf{x}_0)\eta_0 \tag{5}$$

If we now substitute (5) into (2) we obtain the following expression for the Lyapunov exponent,

$$
\begin{aligned}
\lambda &= \lim_{t\to\infty} \frac{1}{t} \ln \left| \mathbf{J}^t(\mathbf{x}_0) \frac{\eta_0}{|\eta_0|} \right| \\
&= \lim_{t\to\infty} \frac{1}{2t} \ln \left| \eta_0^\dagger \left(\mathbf{J}^t\right)^\dagger \mathbf{J}^t \eta_0 \right| \qquad (6)
\end{aligned}
$$

where the normalisation of the η_0 is dropped since $\lim_{t\to\infty} -1/t \ln|\eta_0| = 0$ Using the expression above the Lyapunov exponent is easily found once we know how to integrate the Jacobian matrix numerically. The Jacobian matrix is easily shown to satisfy the equation,

$$
\frac{d}{dt}\mathbf{J}^t(\mathbf{x}) = \mathbf{Dv}(\mathbf{x})\mathbf{J}^t(\mathbf{x}), \qquad \text{with } \mathbf{J}^0(\mathbf{x}) = \mathbf{1} \qquad (7)
$$

where $\left(\mathbf{Dv}(\mathbf{x})\right)_{ij} = \partial v_i(\mathbf{x})/\partial x_j$. Note that the Jacobian matrix satisfies a system of equations similarly to the trajectories and therefore is calculated by the Runge-Kutta algorithm too. For practical purposes we cannot go to the infinite time limit of (6) therefore attention is paid to the asymptotic behaviour, i.e. we plot $1/2 \ln|\eta_0^\dagger \left(\mathbf{J}^t\right)^\dagger \mathbf{J}^t \eta_0|$ versus time.

The Lyapunov exponent defined above is associated to the largest absolute valued eigenvalue of the Jacobian matrix, but actually there is an exponent for each eigenvalue Λ_i^t. The largest eigenvalue, however, will be the dominating when the system evolves. This is clarified by the following expansion, where $\{\mathbf{u}_1, \ldots, \mathbf{u}_d\}$ denotes the eigenvectors of the symmetric matrix $\left(\mathbf{J}^t\right)^\dagger \mathbf{J}^t$ and $\eta_0 = \sum \eta_0^i \mathbf{u}_i$,

$$
\begin{aligned}
\eta_0^\dagger \left(\mathbf{J}^t\right)^\dagger \mathbf{J}^t \eta_0 &= \sum |\eta_0^i \Lambda_i^t|^2 \\
&\approx \sum |\eta_0^i|^2 e^{2\lambda_i t} \qquad (8)
\end{aligned}
$$

where the last approximation is brought about by the asymptotic behavior $\ln|(\mathbf{u}_i)^\dagger \left(\mathbf{J}^t\right)^\dagger \mathbf{J}^t \mathbf{u}_i| \sim 2\lambda_i t$. We see that the largest Lyapunov exponent dominates the latter sum of (8) as long as η_0 is not perpendicular to the dominating eigen direction.

Below the leading Lyapunov exponent of the Rössler system is found and the non-leading exponents are found in connection with periodic orbits only.

The Rössler system is given by the following system of coupled non-linear equations

$$
\begin{aligned}
\dot{x} &= -y - z \\
\dot{y} &= x + ay \\
\dot{z} &= b + z(x - c)
\end{aligned}
$$

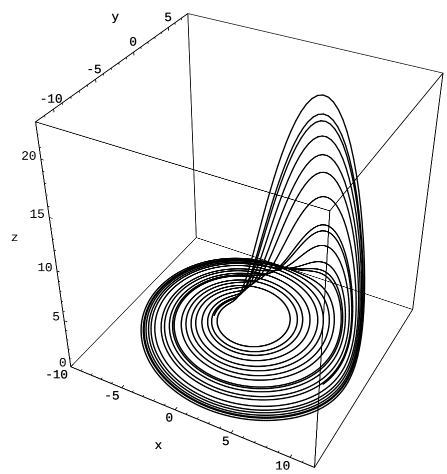

Figure 1: *The Rössler attractor based on one solution curve to the equation system. The reason why the attractor is approximated by a single trajectory is due to the assumption that the attractor has a dense set of initial points that brings a generic trajectory about. A generic trajectory is dense on the attractor.*

Note that the system includes one nonlinear term only, the quadratic term zx, and therefore is one of the simplest systems with chaotic behaviour. Though the equations are simple much effort is still needed to understand the underlying dynamics of the system. In the present text the values $a = b = 0.2$ and $c = 5.7$ are used. These values show by numerically integration that the system has a *strange* attractor, i.e. a fractal attractor.

Figure 2 shows cross sections of the Rössler attractor at various angles and how two initial points are stretched apart and afterwards folded back, similar to the baker's map. The stretch and fold property in particular is what causes the attractor to be fractal.

Figure 3 shows a plot of $1/2 \ln |\eta_0^\dagger \left(\mathbf{J}^t\right)^\dagger \mathbf{J}^t \eta_0|$ versus time, i.e. a plot for estimating the Lyapunov exponent. As the plot shows the temporal dependence is not exactly a straight line, small oscillations and larger humps appear. The small oscillations are due to minor variations in the stretching, i.e. the stretching power fluctuates locally. The larger hump, the sudden fall to a low level, is caused by the spatial limits of the attractor, two trajectories cannot separate further than the spatial extent of the attractor and therefore such a fall is generated when the trajectories suddenly are folded close together.

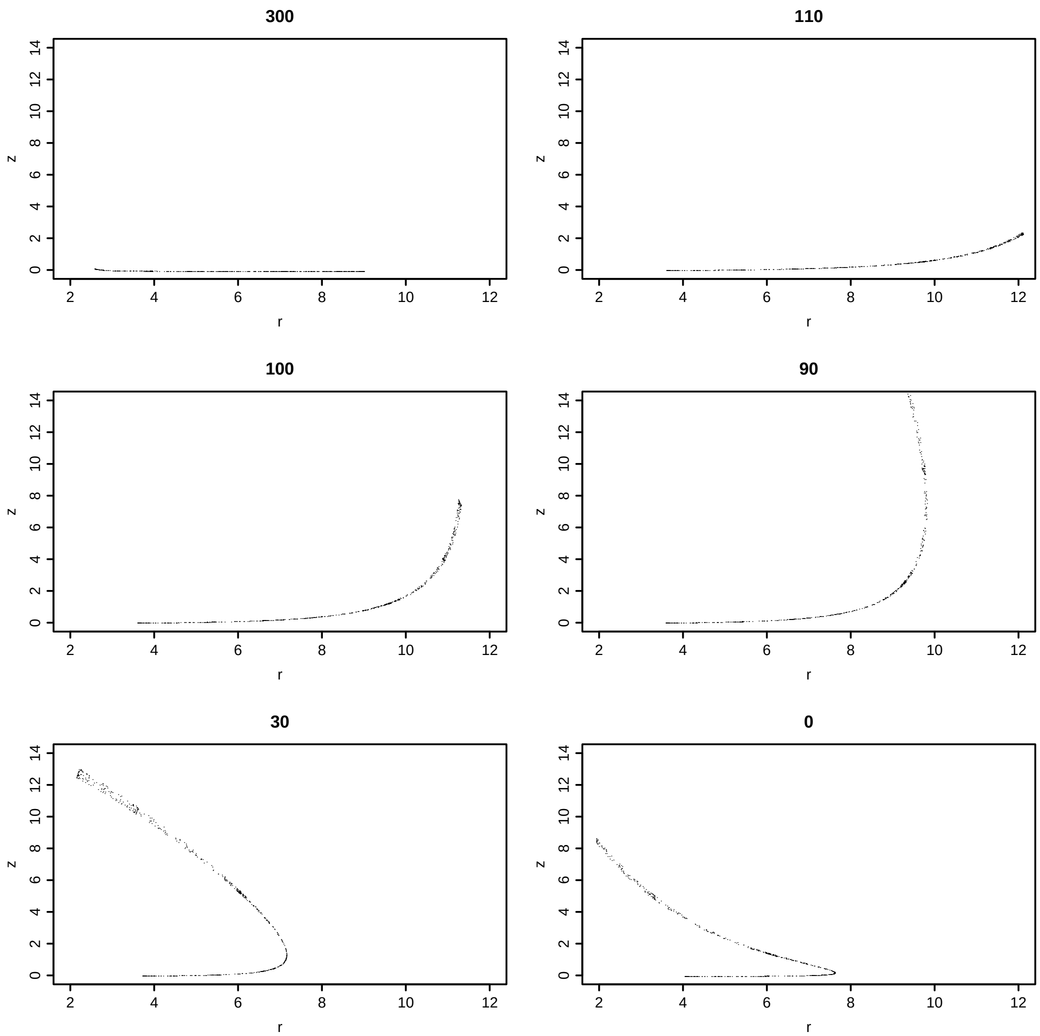

Figure 2: *The figure shows cross sections in cylindrical coordinate at six different angles, where the xy-plane is measured in polar coordinates. The angles relatively to the x-axis are written as title of the plots. The first plot at* $300°$ *shows the unstretched line - the dough used to knead pastry. As we go through the plots the dough is stretched (nearby trajectories separate), folded and then compressed back into a line. The stretch and fold leaves us with a cantor set of surfaces, but since the compressing in the Rössler system is very effective (crunchy pastry) we cannot see traces of the cantor set. Note that we cut a little of the graph at* $90°$ *since it extended to 18.5. The leading Lyapunov exponent is a measure of how fast two nearby trajectories separate, the effectiveness of the stretching.*

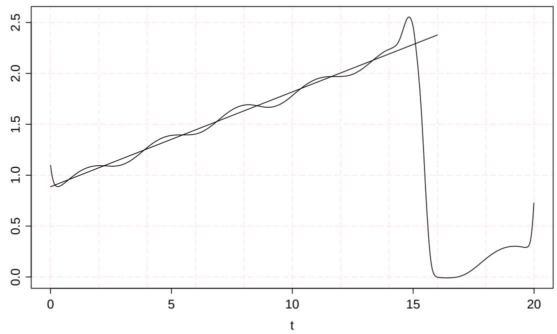

Figure 3: *Plot used for calculating the Lyapunov exponent of the Rössler attractor. We see that the almost straight part of the curve turns in to a sudden fall, and afterwards resumes to increase with an almost linear growth equal to the preceding. If the graph was continued intervals of growth equal to the Lyapunov exponent and humps would alternately appear.*

The almost straight part of the curve is the part of interest and we therefore use it as an estimate of the Lyapunov exponent by fitting it with a straight line. The Lyapunov exponent for the Rössler system assumes the value 0.09 and the positive value makes the attractor unstable, i.e. nearby trajectories separate.

1.2 Return Maps

We shall now focus on relating the three dimensional flow to a one dimensional map. Such a relation will simplify much of the work on the flow since maps generally are more accessible, therefore maps are the subject of the subsequent sections. First step in building up such a relation is to make a cross section Ω of the flow, in particular we choose the set,

$$\Omega = \{(x, y, z) | x = 0, y > 0\} \tag{9}$$

Figure 1 shows that the trajectories are not tangent to Ω (thus the cross section is called a Poincaré section) and after some time τ_y an initial point $y \in \Omega$ will return to Ω, $\phi^{\tau_y}(y) \in \Omega$, where the time of return is a function of y. We can now reduce the flow to a map by the following function f_Ω,

$$y_{n+1} = f_\Omega(y_n) \equiv \phi^{\tau_{y_n}}(y_n), \quad y_n, y_{n+1} \in \Omega \tag{10}$$

The function f_Ω is called a *return map* with respect to Ω . The present Ω is the only cross section used and therefore we omit the subscript Ω on f_Ω.

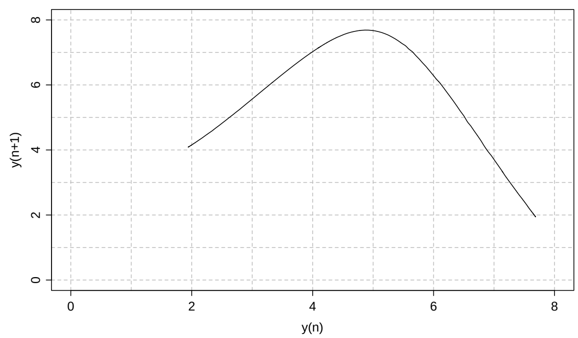

Figure 4: *Return map on the cross section* $\{(x, y, z)|x = 0, y \geq 0\}$.

Figure 4 shows the return map for the Rössler system using Ω and ignoring the z-coordinate. The shape is almost unimodular, i.e. the map has a strictly increasing branch on an interval $[a; c)$, a turning point called the critical point c and a strictly decreasing branch on $(c; b]$, but a unimodular map ought to have the same functional value for a and b. Our return map does not meet the last criterion. With a little imagination, however, we extend the left hand, respectively the right hand branch, such that they both reach the horizontal axis. Our imagination will not change the dynamics of the system, we rather attach extensions to domains where the system does not come as long as the transient part of the trajectories is omitted. The transient part is the part traced before getting sufficiently close to the attractor. In fact, the transient part adds single points outside the smooth curve of the return map, the points vary as we change the initial value of the z-coordinate, and hence a unimodular map is generally not obtained by including a large number of transient trajectories. Therefore it only makes sense to ignore the z-coordinate after the transient trajectory, and use one generic trajectory only. The unimodularity mirrors the stretch and fold behaviour shown in figure 2, the stretch brings the strictly monotone parts of the unimodular map about and the folding separates the map in increasing and decreasing branches, analogous to the behaviour seen in many known chaotic systems such as the baker's transformation.

In practice the return maps were constructed by making a file of 3000 returning-points of a generic trajectory, excluding the transient part. Since the file of returning points is limited the return map varies with the initial point and the number of returns of the construction trajectory. Furthermore the finite integration precision causes the trajectories alternately to move away from and approach the attractor, therefore some small glitches occur on the return map. However the attraction is so strong that we for practical purposes get a reliable return map simply by applying a local interpolation, i.e. the glitches have little spatial extent. Particularly we used a quadratic interpolation, but did also try a local quadratic estimate; both approaches gave the same result for the present purpose. The return map In section 2.1 we will show the return map is significant for statements about the flow.

1.3 Periodic Orbits

Periodic orbit An orbit is said to be periodic if there is a point $\mathbf{x}$ and a time T such that $\phi^T(\mathbf{x}) = \mathbf{x}$ and $\phi^t(\mathbf{x}) \neq \mathbf{x}$ for $0 < t < T$. The periodic orbit is given by the set $\{\phi^t(\mathbf{x}) | 0 \leq t \leq T\}$.

In the search for periodic orbits a Poincaré section is used as basis for the initial points, we choose the Ω defined above. The topological length n of a periodic orbit denotes the number of times a trajectory has hit the Poincaré section when returning to the initial point $\mathbf{x}$ for the first time. The technique used for finding periodic orbits of topological length n was Newton's method implemented with multi point shooting. The multi point shooting was very efficient[1], whenever we were able to come up with a good initial guess of points included in the orbit. To help making good guesses we used the return map and the symbolic dynamics described below. In section A we tabulate characteristics of the periodic orbits up to topological length 7. The Lyapunov exponents of periodic orbits result from integrating the Jacobian matrix around the orbit and then use the eigenvalues Λ_i, found after run, in the expression,

$$\lambda_i = \frac{1}{T_p} \ln |\Lambda_i| \tag{11}$$

In general the periodic orbits of the Rössler system has one expanding direction $|\Lambda_e| > 1$ one contracting $|\Lambda_c| < 1$ and one marginal direction $|\Lambda_m| = 1$, hence the periodic orbits are all unstable. As an example consider the figures shown below. The figures are projections of the periodic orbits on the xy-plane, and show a period one, two and three orbit respectively. The vertical line is the projection of the return map and the symbols are used in the subsequent section. On the left are the corresponding eigenvalues tabulated together with the leading Lyapunov exponent.

---

[1]Efficient means that the algorithm converges fast, and not that the time used to program the algorithm was efficient. Indeed the efficiency for programming the algorithm seemed to be non polynomially (exponentially).

Λ_m	1.000000000006
Λ_e	-2.403953531827
Λ_c	-1.287858708564E-14
λ_e	0.149141556638

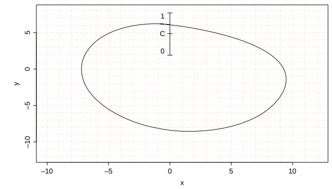

Λ_m	1.000000000114
Λ_e	-3.512006981516
Λ_c	1.658641011821E-17
λ_e	0.106831136551

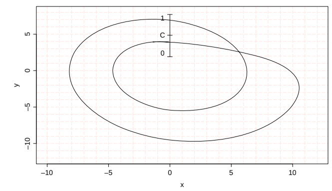

Λ_m	1.000000000686
Λ_e	-2.341923503691
Λ_c	-2.748210188065E-13
λ_e	0.048583166951

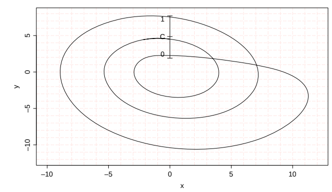

The estimation of the contracting eigenvalue is quite difficult, since it changes dramatically with the precision used for calculations. Figure 5 shows the size of the contracting eigenvalue from the period one orbit as the precision changes from floating points ($\sim 10^{-6}$) to double precision ($\sim 10^{-16}$). We see that floating points are insufficient for estimation, and double precisions might give a clue about the order of the eigenvalue ($\sim 10^{-14}$). Other factors such as the integration step size (dt=0.00001) have influence on the calculations so we are not directly able to conclude on basis of the figure.

2 Admissible Orbits

2.1 Symbolic Dynamics

This section introduces symbolic dynamic as used in the subsequent kneading theory.

Symbolic dynamics denotes a particular class of dynamical systems, which is very useful when modelling smooth and hence more complicated systems. Take the return map above as an example. We will now code it, using a ternary alphabet $\mathcal{A} = \{0, \frac{1}{2}, 1\}$, where $x_{n+1} = f(x_n)$ denotes the return map.

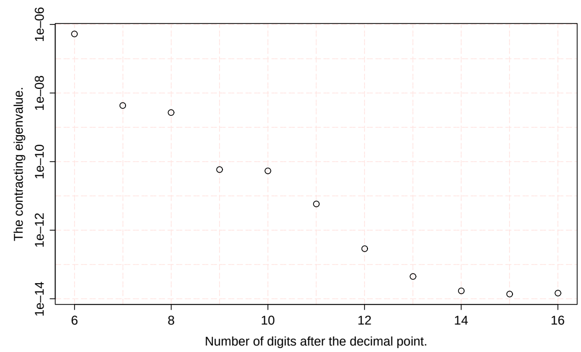

Figure 5: *The contracting eigenvalue plotted versus the number of decimals used through the calculations.*

The interval $\mathcal{M}$, on which f is defined, is separated in two disjoint intervals $\mathcal{M}_0$ and $\mathcal{M}_1$. These are the intervals where f increases and decreases respectively. The letter $\frac{1}{2}$ is introduced as symbol for the critical point $x_c = \mathcal{M}_{\frac{1}{2}}$, though it is a little beside standard notation it is useful as we shall see in the subsequent section. The dynamics $x_0, f(x_0), f^2(x_0), \ldots = x_0x_1x_2\ldots$ is coded by symbols $s_0s_1s_2\ldots$ using the recipe

$$s_n = \begin{cases} 0, \; x_n \in \mathcal{M}_0 \\ \frac{1}{2}, \; x_n = x_c \\ 1, \; x_n \in \mathcal{M}_1 \end{cases}$$

To each initial point $x_0 \in \mathcal{M}$ we associate a symbolic sequence by the map

$$x_0x_1x_2\ldots \mapsto s_0s_1s_2,\ldots, \qquad S^+(x_0) = s_0s_1s_2\ldots.$$

$S^+(x_0)$ is called the itinerary of x_0, where the superscript $+$ indicates that the symbolic sequence specifies the future dynamic, i.e. the behavior succeeding the initial point. We cannot make a past itinerary since the dynamic is not invertible; the return map is surjective. A finite sequence of symbols from our alphabet is called a block, and a block $s_i, s_{i+1}, \ldots, s_{i+n}$ is allowed by our dynamical system if

$$\bigcap_{j=1}^{n} f^{-j}(\mathcal{M}_{s_{i+j}}) \neq \emptyset$$

Consider as an example the block 1000, which is forbidden, due to the sub-block of three zeros. Why three zeros in succession are forbidden either can be seen by the intersection of sets above or by the geometrical argument given in figure 6.

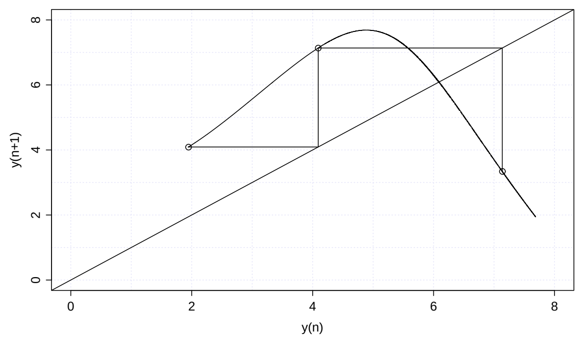

Figure 6: *From the figure we see it is not possible to obtain a block with more than two zeros in succession, since all trajectories will intersect values greater or equal to the plotted piece of a trajectory, thus the block 1000 is forbidden in the Rössler system.*

A symbolic sequence is called *admissible* if it contains no forbidden blocks, otherwise it is *inadmissible*. We denote the subset of admissible symbolic sequences of all symbolic sequences by $\Sigma = \{\alpha \in \mathcal{A}^{\{0,1,2,3\ldots\}} | \alpha \text{ is admissible}\}$, the subset is called a *subshift*. Finally we put in some dynamics to our symbolic system by introducing the *shift operator* σ,

$$\sigma(s_0 s_1 s_2 \ldots) = s_1 s_2 s_3 \ldots$$

Note that the subshift is invariant to the shift operator, since a block $s_1 \ldots s_n$ remains allowed though its first symbol is removed,

$$\bigcap_{j=1}^{n} f^{-j}(\mathcal{M}_{s_j}) \neq \emptyset \quad \Rightarrow \quad \bigcap_{j=2}^{n} f^{-(j-1)}(\mathcal{M}_{s_j}) \neq \emptyset. \tag{12}$$

The implication follows from the fact that $f(\mathcal{M}_a \cap \mathcal{M}_b) \subseteq f(\mathcal{M}_a) \cap f(\mathcal{M}_b)$ and if $f^{-n}(\mathcal{M}_a) \cap f^{-m}(\mathcal{M}_b) \neq \emptyset$ then

$$\emptyset \neq f\big(f^{-n}(\mathcal{M}_a) \cap f^{-m}(\mathcal{M}_b)\big) \subseteq f^{-(n-1)}(\mathcal{M}_a) \cap f^{-(m-1)}(\mathcal{M}_b).$$

Therefore the evolution of the system does not go from being admissible to inadmissible by making a time step ahead.

The point about symbolic dynamics might be put into a single equality, which is due to its conjugacy to the original dynamics,

$$\sigma \circ S^{+}(x) = S^{+} \circ f(x)$$

However the dynamical systems might not be completely conjugate, depending on whether S^+ is surjective only or bijective. Anyway, S^+ is our way to relate the two points of viewing the dynamics.

From these more mathematical details we return to the present concern about the Rössler system. The new way of seeing the system equips us with a very useful shorthand notation for periodic orbits. Consider for instance the periodic orbits shown in figure 7. These periodic orbits are named after their path in the system, for instance are the period two orbit named $010101\ldots$ if it starts in the left and increasing part of the return map and $101010\ldots$ if the right part. The names are abbreviated using a overline, i.e. $010101\ldots = \overline{01}$. In particular the two period two orbits are just two sides of the same part, hence they are considered equal. Likewise we do the same identification to the period three orbits $\overline{001}, \overline{010}$ and $\overline{100}$, and in general each shift of a periodic orbit is represented with the same cycle - namely the prime cycle. An important property about the symbolic names for the periodic orbits is

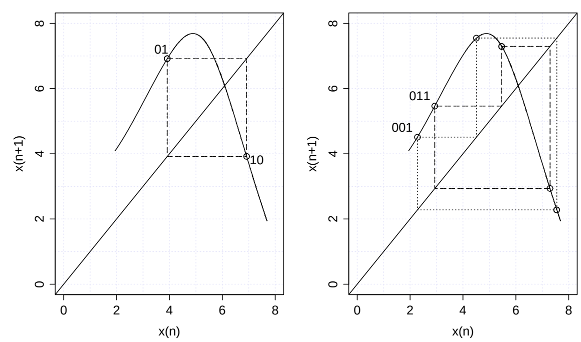

Figure 7: *The period two and the period three orbits of the Rössler system respectively. The drawn orbits are the one dimensional versions of the orbits sketched in the preceding section.*

the uniqueness of the names when considering maps like the present, hence no more than one period two orbit occurs with the name $\overline{01}$.

From the preceding remarks and figure 6 we should not expect to find the periodic orbit $\overline{0001}$ since it contains the forbidden block 1000. Next section introduces an effective way to find admissible periodic orbits, orbits without forbidden blocks.

2.2 Kneading Theory

In the preceding chapter we saw that some orbits (itineraries) seemed inadmissible by our dynamical system, but no quantification of the word admissible was achieved, however. The kneading theory, walked through below, turns out to be very useful for such a quantification.

The idea is to find an ordering of our shift space and put up a border, regarding the ordering, between admissible and inadmissible itineraries. Admissible orbits are then found on one side of the border and inadmissible on the other. The border is brought about, as we shall see, by considering the symbolic encoding of the critical point.

Kneading sequence and value, let x_c denote the critical point of a unimodular map, then the kneading sequence K is equal to the future itinerary of $f(x_c)$,

$$K = S^+\big(f(x_c)\big).$$

Figure 8 shows the first 9 iterations of the critical point, and it has the kneading sequence,

$$K_{Rössler} = 1001011111111010110010\ldots \tag{13}$$

Note that the cobwebbing after 5 iterations is getting nearby the fixed point $(\overline{1})$, and therefore stays in the neighbourhood for a while, i.e. we obtain the shown block of ones.

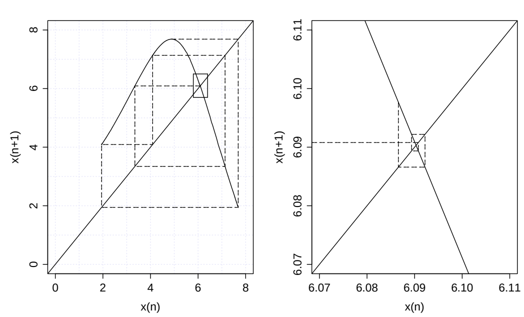

Figure 8: *Kneading sequence of our Rössler return map. The right figure shows a zoom on the fixpoint.*

Next we define an ordering (Katok,[2]) on our shift space Σ. Let $\alpha, \beta \in \Sigma$ be two itineraries, then we denote $\alpha \prec \beta$ if there exists an n such that $\alpha_i = \beta_i$

for $1 \leq i < n$ and

$$\Big((1-2\alpha_1)\cdots(1-2\alpha_{n-1})\Big)(1+\alpha_n) < \Big((1-2\beta_1)\cdots(1-2\beta_{n-1})\Big)(1+\beta_n) \tag{14}$$

Note that the product $(1-2\alpha_0)\cdots(1-2\alpha_{n-1})$ either has absolute value one or equals zero. The latter case occurs when $\sigma_1^i(\alpha) = \frac{1}{2}$ for some $0 \leq i < n$, and in particular for that case $\sigma^{i+1}(\alpha) = \sigma^{i+1}(\beta) = K$. If α equals the itinerary $S^+(x_0)$ of an initial point x_0, the sign in the former case tells us, whether $f^n(x_0)$ is increasing or decreasing, since

$$\begin{aligned} sign\big((f^n)'(x_0)\big) &= sign(f'(x_0)f'(x_1)\cdots f'(x_{n-1})) \\ &= (1-2\alpha_1)\cdots(1-2\alpha_{n-1}) \end{aligned} \tag{15}$$

Where the last expression is brought about by the properties of our symbolic coding, see section 2.1.

Let x_0 and y_0 denote two initial points where $S^+(x_0) \prec S^+(y_0)$. We will now show that $x_0 < y_0$. First we notice that the future itineraries, in order to satisfy (14), not will assume the value $\frac{1}{2}$ at the first (n-1)'th tuplets, since we then would obtain equality. Moreover is $S_i^+(x_0) = S_i^+(y_0)$ for $1 \leq i < n$ and $S_n^+(x_0) \neq S_n^+(y_0)$. We consider the two possibilities of sign of $(f^n)'$ separately. If the sign is positive, i.e. $f^n(x)$ increases on an interval containing x_0 and y_0, we have that,

$$\begin{aligned} &\Big((1-2S_1^+(x_0))\cdots(1-2S_{n-1}^+(x_0))\Big)(1+S_n^+(x_0)) \\ < \;&\Big((1-2S_1^+(y_0))\cdots(1-2S_{n-1}^+(y_0))\Big)(1+S_n^+(y_0)) \end{aligned}$$

which implies,

$$S_n^+(x_0) < S_n^+(y_0)$$

Therefore the itinerary of x_0 has a "smaller" symbolic value at n tuplet than y_0, and consequently $f^n(x_0) < f^n(y_0)$. Since f^n is increasing on an interval containing x_0 and y_0 we have $x_0 < y_0$. A similar argument applies for the case when f^n is decreasing, and once more we obtain $x_0 < y_0$. We then managed to see the coordinates follow the ordering invoked on the shift space.

Subsequently we might contrapose the argument to achieve the result, $x_0 < y_0$ implies $S^+(x_0) \preceq S^+(y_0)$. Particularly, the contraposed argument tells us that the ordering on our shift space follows the ordering of the coordinate space but not strictly, in other words an interval of coordinates might result in the same itinerary.

The point that makes the shift space ordering above useful is its relation to the standard ordering of the real numbers[2], the ordering is "preserved" (almost). We know, from the return map, that our dynamical system is forbidden to assume values above $f(x_c)$, i.e. $f^k(x) \leq f(x_c)$, $k \in \mathbb{N}$. If the system after some n iterations equals the critical value then the itinerary shifted by σ^n equals the kneading sequence $\sigma^n(S^+(x)) = S^+(f^n(x)) = S^+(f(x_c)) = K$, otherwise we have strict inequality, $f^k(x) < f(x_c)$, hence $S^+(f^k(x)) \preceq S^+(f(x_c)) = K$, $k \in \mathbb{N}$. So a necessary condition for an itinerary S^+ to be admissible is $\sigma^k(S^+) \preceq K$, $k \in \mathbb{N}$. Actually the condition is sufficient for the strict ordering (Katok, [2]),

Admissibility. If $\alpha \in \Sigma$ is a symbol sequence and $\sigma^i(\alpha) \prec K$ for all $i \geq 0$ then there exists an initial point x such that $\alpha = S^+(x)$.

Now we have a tool for extracting the admissible orbits of the Rössler attractor, and it is very easily applied indeed. For instance are the periodic orbit $\overline{0001}$ inadmissible, since $\sigma^3(\overline{0001}) = 10001000100\ldots \not\prec 10010111111\ldots = K$. The technique for fast comparison of two symbolic sequences is to count the number of ones appearing in the sequences before they have a non-equal tuplet. If the number of ones is even or odd and the first non-equal tuplets are the n'th then

$$\alpha_n < \beta_n \Rightarrow \begin{cases} \alpha \prec \beta, \text{ if } \sum_{i=1}^{n-1} \alpha_i \text{ is even.} \\ \alpha \succ \beta, \text{ if } \sum_{i=1}^{n-1} \alpha_i \text{ is odd.} \end{cases}$$

The technique for comparing symbolic sequences was implemented on a computer which quickly found that the following prime cycles up to topological length 10 are admissible for the Rössler system,

n_p	p					
1						$\overline{1}$
2						$\overline{01}$
3					$\overline{001}$	$\overline{011}$
4						$\overline{0111}$
5					$\overline{01011}$	$\overline{01111}$
6				$\overline{001011}$	$\overline{010111}$	$\overline{011111}$
7		$\overline{0101011}$	$\overline{0110111}$		$\overline{0101111}$	$\overline{0111111}$
8	$\overline{01011011}$	$\overline{01010111}$	$\overline{01101111}$	$\overline{00101111}$	$\overline{01011111}$	$\overline{01111111}$
						$\overline{00101101}$
9	$\overline{010110111}$	$\overline{010101111}$	$\overline{011011111}$	$\overline{001011011}$	$\overline{010111111}$	$\overline{011111111}$
			$\overline{011010111}$	$\overline{011101111}$	$\overline{001001011}$	$\overline{010101011}$
10	$\overline{0101101111}$	$\overline{0101011111}$	$\overline{0110111111}$	$\overline{0010111111}$	$\overline{0101111111}$	$\overline{0111111111}$
	$\overline{0101111011}$	$\overline{0101110111}$	$\overline{0110110111}$	$\overline{0111011111}$	$\overline{0101011011}$	$\overline{0101010111}$
			$\overline{0010110111}$	$\overline{0010110101}$	$\overline{0010111101}$	$\overline{0010110111}$

[2]In mathematical terms we could make the relation of the two orderings strict by partitioning the real numbers in equivalence classes, where an equivalence class associated to a number x is the set $\{y|S^+(y) = S^+(x)\}$, then $x < y \Leftrightarrow S^+(x) \prec S^+(y)$.

2.3 How to Find the Kneading Sequence?

The kneading sequence (13) was estimated regarding it as a function of the integration time step and the number of returns of the construction trajectory. For a selected set of integration times the corresponding return map was calculated and thereafter the kneading sequence was found. The return map in each case was based on a generic trajectory having 4000 returns.

As we decrease the time step we expect to get closer to the true orbit as well as getting a better return map. Therefore the correction for each decrement is expected to grow negligible and in particular fast enough for convergence. The table below shows the kneading sequences $K_{\Delta t}$ as function of the time step Δt,

$$\begin{array}{lcl}
K_{.1} & = & 10010111111\mathit{0110010111} \\
K_{.05} & = & 100101111111\mathit{101001011} \\
K_{.01} & = & 100101111111010\mathit{010010} \\
K_{.005} & = & 100101111111010110\mathit{110} \\
K_{.001} & = & 100101111111010110010 \\
K_{.0005} & = & 100101111111010110010 \\
K_{.0001} & = & 100101111111010110010
\end{array}$$

Within our finite precision the kneading sequence seems to converge and therefore we take $K_{.0001}$ as the estimate used throughout the present text. This kneading sequence was actually confirmed by $K_{.01}$ and 10000 returns since they both agreed on the first 21 tuplets. The tendency was that for large integration time steps the inaccuracy was averaged out by demanding a larger number of returns.

The kneading sequence behavior for various timesteps are moreover demonstrated in the extraction of the topological ζ-functions, see figure 11.

3 ζ-functions

3.1 Cycle Expansions and Shadowing

The subsequent sections will not go in to theoretical details about the ζ-function but restrict themselves to use of the ζ-function's tremendous applicability. For the present purpose the ζ-function is expressed in the *Euler* *product representation*

$$1/\zeta = \prod_p (1 - t_p), \quad \text{where } t_p = \frac{1}{|\Lambda_p|} e^{\beta n_p} z^{n_p} \tag{16}$$

The ζ-function for the Rössler system is a polynomial of the unbounded order z^{n_p}, and might be expanded in increasing order as shown in the table below, where we tabulate the admissible prime orbits up to order 6,

n_p	Cycle expansion
0	1
1	$-t_1$
2	$-t_{01}$
3	$-(t_{011} - t_{01}t_1) - t_{001}$
4	$-(t_{0111} - t_{011}t_1) + t_{001}t_1$
5	$-(t_{01011} - t_{011}t_{01}) - (t_{01111} - t_{0111}t_1) + t_{001}t_{01}$
6	$-(t_{001011} - t_{011}t_{001} + t_{001}t_{01}t_1) - (t_{010111} - t_{01}t_{0111}) - (t_{011111} - t_{01111}t_1)$
	$-(t_{01}t_{011}t_1 - t_{01011}t_1)$

Some terms are *shadowed* by products of lower order terms, and the shadowing, indeed, makes the ζ-function useful. The infinite product generating the ζ-function would be awkward to handle if it converged slowly, but the individual terms are almost matched by their shadow and gaurentees fast convergence by use of a finite cycle length truncations. Some terms, however, remains unshadowed and to check the convergence we make a test of quality of the finite truncation. Trajectories in the Rössler system are confined for infinite times, the flow is conservated, hence the fraction of trajectories leaving the system (the escape rate) equals zero. The ζ-function mirrors the vanishing escape rate by satisfying (chapter 12.1 of [1]),

$$\frac{1}{\zeta(1)} = 0 \tag{17}$$

The quality test is to see how the truncated ζ-function ζ_N (expanded to polynomial order N) satisfies the equality above as a function of N. Figure 9 shows the result.

Moreover stability ordering was applied on the cycle expansions (chapter 10.5 of [1]), i.e. the shadows (pseudocycles) were ordered with respect to some maximal stability value, e.g. the absolute value of the maximal expanding eigenvalue of the data set, and all pseudocycles having a product of expanding eigenvalues exceeding this maximum were dropped. Using the stability ordering brings almost the same results about as the results found by use of the ordering in the table above (see below).

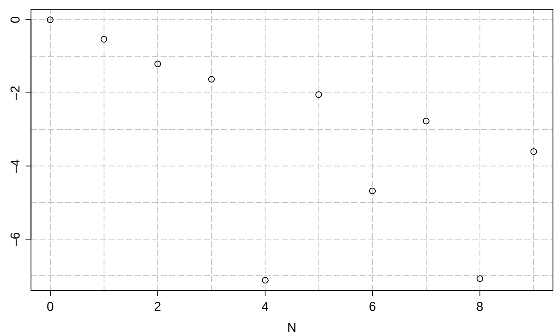

Figure 9: $\log \zeta_N(1)$ *versus* N. *Though we have few observation points the tendency is obvious the convergence seems exponentially, and we should expect to come up with a useful result by applying the cycle expansion.*

We will now focus on the return map and its topological ζ-function.

Unimodal maps like the present return map do have a remarkable simple expansion rule of its topological ζ-function. The expansion is given in terms of the kneading sequence, the border between admissible and inadmissible orbits, and explicitly written as (chapter B.2 of [1])

$$\frac{1}{\zeta(z)} = \prod_p (1 - z^{n_p}) = (1 - z) \sum_{i=0}^{\infty} a_i z^i, \quad a_i = \prod_{j=1}^{i} (-1)^{K_j} \tag{18}$$

where $a_0 = 1$ and K_j denotes the value of the j'th tuplet of the kneading sequence K. The expansion as written above assumes that the kneading sequence is non-periodic. For periodic orbits of topological length n, ∞ is substituted with $n - 1$. The expansion rule for our estimated and probably non-periodic kneading sequence tells us to evaluate an infinite sum, but we are only capable of approximating by a finite number of the lowest order terms. Fortunately is the convergence, by adding terms of higher order successively, fast and with the limited kneading sequence we are enabled to estimate the topological entropy with good precision. The leading root z_0 of the ζ-function is related to the topological entropy trough, $z_0 = e^{-h}$.

Plugging the kneading sequence (13) into (18) leads to the following truncated inverse topological ζ-function,

$$\begin{aligned} 1/\zeta_{21}(z) = {} & 1 - z - z^2 - z^3 + z^4 + z^5 - z^6 + z^7 \\ & - z^8 + z^9 - z^{10} + z^{11} - z^{12} - z^{13} + z^{14} + z^{15} \\ & - z^{16} + z^{17} + z^{18} + z^{19} - z^{20} - z^{21} \end{aligned} \tag{19}$$

which has the leading root $0.6006432\ldots$, hence the topological entropy,

$$h = -\log 0.600643\ldots = .50975\ldots$$

The leading root above is the best estimate allowed by the kneading sequence at hand and figure 10 shows how the logarithmic distance of the leading root to the best estimate varies as we include more and more terms in the polynomial expansion, and indeed the truncation approximations are converging fast, exponentially. Figure 11 shows a double logarithmic plot of how the

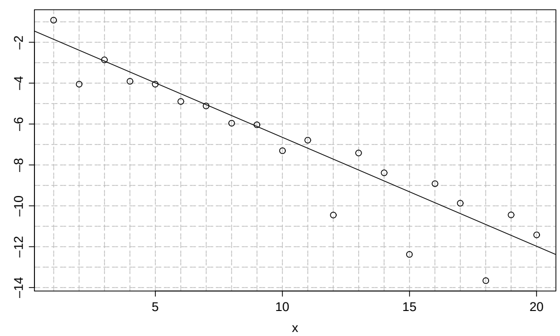

Figure 10: *Plot of the logarithm distance between the leading root and the best estimate as a function of the polynomial versus order.*

leading root of $1/\zeta_{21}$ changes in logarithmic distance to the best estimate as the integration time step is varied. The convergence seems to be polynomial of the approximately order 6, and hence quite fast as the time steps decreases. The almost monotone behaviour of the points confirms that by decreasing the time steps the kneading sequence converges.

3.2 The Lyapunov Exponent

We will now find the Lyapunov exponent of the returmap using two different approaches.

The first approach is in principle similar to the approach in section 1.1, for 1-d maps, the logarithmic distance of two initially nearby trajectories are plotted as function of the number of iterations. The slope of the estimated line through the resulting distances is the Lyapunov exponent of the return map, and it assumes the value $\underline{\underline{\lambda_{rm} \approx 0.42}}$.

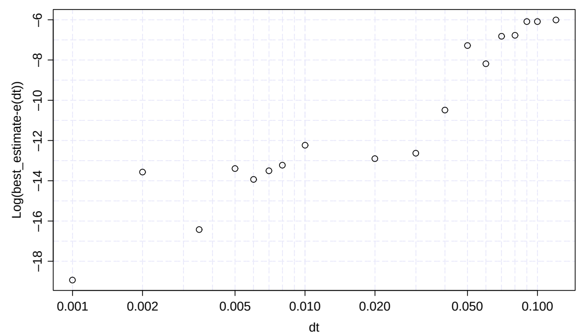

Figure 11: *Logaritmic distance to the best estimate of the leading root versus the integration time step.*

The second approach is to consider the Lyapunov exponent as the dynamical average of the local divergence rate $\lambda(x) = \log|f(x)'|$. The average results from the cycle averaging formula (chapter 10.2.1 and 12.2.1 of [1]),

$$\lambda_{rm} = \frac{1}{\langle n \rangle_\zeta} \sum_\pi (-1)^{k+1} \frac{\log|\Lambda_{p_1}| + \cdots + \log|\Lambda_{p_k}|}{|\Lambda_{p_1} \cdots \Lambda_{p_k}|} \tag{20}$$

where the cycle mean of n is found from

$$\langle n \rangle_\zeta = \sum_\pi (-1)^{k+1} \frac{n_{p_1} + \cdots + n_{p_k}}{|\Lambda_{p_1} \cdots \Lambda p_k|}. \tag{21}$$

If we plug in the data set from the table in section A to the formulas above the Lyapunov exponent assumes the value $\underline{\underline{\lambda_{rm} \approx 0.43}}$. Figure 12 shows the logarithmic distance to 0.43 as function of the truncation N, and as in the case of the flow conservation test the behaviour seems exponentially convergent.

The particular reader might have noticed that the present Lyapunov exponents are not equal to the estimate given in section 1.1, where we found the flow exponent $\lambda_f \approx 0.09$. They are not supposed to be equal, since going from flows to return maps implies that the time of one return on the flow is set to unity. An infinitesimal distance δy_0 on the return map is increased by a factor $e^{\lambda_{rm}}$ after one iteration,

$$\delta y \approx e^{\lambda_{rm}} \delta y_0$$

contrary to the flow where

$$\delta y \approx \Lambda^{\tau_{yo}} \delta y_0 = e^{\lambda_f \cdot \tau_{yo}} \delta y_0.$$

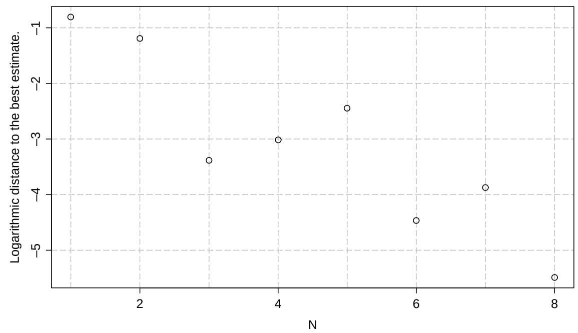

Figure 12: *The figure shows the logarithmic distance to the best estimate found for N=9.*

τ_{y_0} denotes the time of return to the Poincaré section. Therefore the flow and the return map Lyapunov exponents are related through some characteristic time τ_c of one round on the attractor.

$$\lambda_{rm} \approx \tau_c \lambda_f$$

To get an idea of the difference between the two Lyapunov exponents we could use the following fraction as the characteristic time $\tau_c = \langle T \rangle_\zeta / \langle n \rangle_\zeta$, where $\langle T \rangle_\zeta$ is the mean cycle period found by inserting T in (21) and τ_c then is the cycle mean time per cycle mean length. By calculating the means we obtain that $\tau_c \approx 5.81$, hence the values of $\lambda_f \approx 0.09$ and $\lambda_{rm} \approx 0.43$ agrees since $0.43/5.81 \approx 0.07$.

It is a time demanding task to calculate the Lyapunov exponents through the periodic orbit theory, but once the preparations are done, the applicability reaches much farther. For instance is the formula (21) extendable to other observables of the system, and the results achieved so far makes the evaluation a minor task. The elements used for the orbit theory calculations were

- A return map was found.
- The kneading theory was applied to the return map and used to extract the admissible periodic orbits.
- The Newton method was used to find the spatial location of the admissible orbits.
- The stabilities of the individual periodic orbits were calculated by implementing the fourth order Runge-Kutta algorithm.

- The ζ-function was expanded in terms of prime orbit stabilities.
- Finally we used the dynamical ζ-function average.

A Data of the Periodic Orbits

Below we tabulate single points and the expanding eigenvalues of the periodic orbits up to topological length seven. Throughout the text we used periodic orbits up to topological length nine.

n_p	p	$y_{initial}$	$z_{initial}$	Λ_e
1	$\overline{1}$	6.091768319056803	1.299731937639821	-2.4039535318268
2	$\overline{01}$	3.915804049621049	3.692833386542665	-3.5120069815161
3	$\overline{001}$	2.278281031720258	7.416480984019008	-2.3419235232340
	$\overline{011}$	2.932877559129124	5.670805943881501	5.3449081538885
4	$\overline{0111}$	3.466758713211455	4.506217531477667	-16.6967406980700
5	$\overline{01011}$	4.162798782914948	3.303903338609633	-23.1995830097831
	$\overline{01111}$	3.278914359770783	4.890452922955567	36.8863297988981
6	$\overline{001011}$	2.122093931936202	7.886172854283211	-6.8576654190825
	$\overline{010111}$	4.059210605826523	3.462265228606606	61.6490940089068
	$\overline{011111}$	3.361494458061049	4.718206217035575	-92.0825560711089
7	$\overline{0101011}$	3.842769382372052	3.815493592299824	77.7611048852412
	$\overline{0110111}$	3.025956697151134	5.451444475664179	-95.1838846735358
	$\overline{0101111}$	4.102255295518855	3.395643547170646	-142.2379888163439
	$\overline{0111111}$	3.327986189581191	4.787462810306583	218.0283602810993

References

[1] Cvitanović, P., *Classical and Quantum Chaos: A Cyclist Treatise*, http://www.nbi.dk/~dasbuch

[2] Katok, A., Hasselblatt, B. (1995), *Introduction to the Modern Theory of Dynamical Systems*, Cambridge University Press.